J. Membrane Biol. 187, 37–50 (2002)
DOI: 10.1007/s00232-001-0151-9

The Journal of
Membrane
Biology

Evidence for a Central Role for Electro-Osmosis in Fluid Transport by Corneal Endothelium

J.M. Sánchez[1], Y. Li[1], A. Rubashkin[1,5], P. Iserovich[1], Q. Wen[1], J.W. Ruberti[2], R.W. Smith[1], D. Rittenband[1], K. Kuang[1], F.P.J. Diecke[3], J. Fischbarg[4,1]

[1]Department of Ophthalmology, College of Physicians and Surgeons, Columbia University, W 168th St., New York, NY 10032, USA
[2]Department of Biomedical Engineering, Northwestern University, Evanston, IL 60208-3100, USA
[3]Department of Pharmacology and Physiology, UMDNJ, New Jersey Medical School, Newark, NJ 07103-2714, USA
[4]Department of Physiology and Cellular Biophysics, College of Physicians and Surgeons, Columbia University, W 168th St., New York, NY 10032, USA
[5]Institute of Cytology, Saint-Petersburg, Russia

Received: 14 August 2001/Revised: 16 January 2002

Abstract. The mechanism of transepithelial fluid transport remains unclear. The prevailing explanation is that transport of electrolytes across cell membranes results in local concentration gradients and transcellular osmosis. However, when transporting fluid, the corneal endothelium spontaneously generates a locally circulating current of ~25 μA cm^{-2}, and we report here that electrical currents (0 to ±15 μA cm^{-2}) imposed across this layer induce fluid movements linear with the currents. As the imposed currents must be ~98% paracellular, the direction of induced fluid movements and the rapidity with which they follow current imposition (rise time ≤3 sec) is consistent with electro-osmosis driven by sodium movement across the paracellular pathway. The value of the coupling coefficient between current and fluid movements found here (2.37 ± 0.11 μm cm^2 hr^{-1} μA^{-1}) suggests that: 1) the local endothelial current accounts for spontaneous transendothelial fluid transport; 2) the fluid transported becomes isotonically equilibrated. Ca^{++}-free solutions or endothelial damage eliminate the coupling, pointing to the cells and particularly their intercellular junctions as a main site of electro-osmosis. The polycation polylysine, which is expected to affect surface charges, reverses the direction of current-induced fluid movements. Fluid transport is proportional to the electrical resistance of the ambient medium. Taken together, the results suggest that electro-osmosis through the intercellular junctions is the primary process in a sequence of events that results in fluid transport across this preparation.

Correspondence to: J. Fischbarg; email: jf20@columbia.edu

Key words: Electrolytes — Osmosis — Fixed charges — Intercellular junctions — Zeta potential — Electrokinetic potential

Introduction

After the cloning and characterization of aquaporin water channel proteins (Preston et al., 1992), it was observed that, in the kidney, aquaporins were expressed by epithelial cells only in those segments where fluid transfer occurred (Nielsen et al., 1993). This was taken to indicate that aquaporins were conduits for transcellular water flow. In addition, absence of aquaporin 2 function (in a human) led to inability to concentrate urine in vasopressin-dependent fashion (Deen et al., 1994), and absence of aquaporins 1 or 3 in knockout mice led to polyuria and some inability to concentrate urine (Yang, Ma & Verkman, 2001). This reinforced explanations that epithelial fluid transport took place by local osmosis across cell membranes endowed with aquaporins (Spring, 1998). On the other hand, however, absence of aquaporin 1 function (in humans with the Colton null mutation (Mathai et al., 1996)) did not result in appreciable fluid transport pathology (Preston et al., 1994). Similarly, in aquaporin null mice (AQPs 1, 3–5 absent), layers transporting fluid at comparatively slow rates, such as lacrimal glands, showed no compromise in their secretory function (Moore et al., 2000). In a related matter, years ago H. Ussing (Ussing & Eskesen, 1989) examined a model of local osmosis. The question asked was: can an epithelial layer separating two identical solutions generate iso-

tonic transcellular fluid transport? The conclusion was categorically negative. The reason given was that friction between water and the cell contents would always slow down water flow with respect to the electrolyte flow; cells could only secrete hypertonic fluid. Hence, independently of an aquaporin role in some fluid transporting epithelia, there seem to be inconsistencies in the evidence for isotonic fluid transport by transcellular local osmosis across aquaporins. In what follows, we propose a different, novel paradigm for epithelial fluid transport.

In view of the inconsistencies noted, we reassessed the theory of transport of electrolytes in the corneal endothelial layer (although misnamed for historical reasons, this layer is a typical fluid-transporting epithelium). This led us to reexamine some inconclusive results we had previously obtained (Kuang, Cragoe & Fischbarg, 1993) on electro-osmosis through intercellular junctions as a possible explanation for the coupling between electrolyte and water movements.

The idea of a connection between electro-osmosis and fluid secretion has received periodic attention in the literature, beginning with a suggestion by Carl Ludwig in 1850 (as cited by McLaughlin and Mathias (1985)). In 1975, Hill (1975) discussed electro-osmotic fluid transfer across an epithelial model in terms of coupling across its boundary membranes. In 1980, the same author discussed non-osmotic theories to explain fluid flow in leaky epithelia, favoring either electro-kinetic or peristaltic junctional flows (Hill, 1980). McLaughlin and Mathias (1985) modeled the reabsorption of fluid by renal proximal tubules on the basis of electro-osmosis along the lateral intercellular spaces and found that they might account for the observed reabsorption rates. They did not consider electro-osmosis across the tight junctions, including them only in their boundary conditions. They used their model to partially account for fluid movements seen upon imposition of currents across proximal kidney tubules in experiments such as those of Spring and Paganelli (1972). Rae and Mathias (1985) hypothesized that electro-osmosis might play a central role in fluid circulation in the lens, and Pasquale et al., (1990) concluded that electro-osmosis could generate fluid movement into the lens along clefts between fiber cell membranes.

On the subject of electro-osmosis across intercellular junctions, in 1985 Lyslo and colleagues (Lyslo et al., 1985) investigated the role of the electrical potential across corneal endothelium. Remarkably, they proposed that Na^+ secreted basolaterally reenters the cell apically, and that the circulation of Na^+ across the junctions is what drags fluid across the layer. Unfortunately, their report attracted little attention. Later on, Ussing (Ussing & Eskesen, 1989) presented evidence for paracellular fluid flow linked electro-osmotically to a recirculating Na^+ current in frog skin glands. The preparation used was complex, including two different types of cells, but the evidence was intriguing. We examined the matter at the time, and found evidence for the presence of an epithelial Na^+ channel (ENaC) in the corneal endothelium (Kuang et al., 1993). In addition, using a volume clamp method to determine fluid transport across rabbit corneal endothelium, we found that electrical currents across the endothelial preparation induced fluid movements in a way qualitatively consistent with the Lyslo-Ussing arguments (Kuang et al., 1993). However, the currents required to generate physiological levels of fluid flow were somewhat larger than those consistent with ideal isotonic electro-osmosis (Kuang et al., 1993), which prevented a firm interpretation. Still, in a recent paper, Hemlin (1995) described electro-osmotically induced fluid flows across jejunal epithelium. Against this background, we decided to revisit the issue of fluid transport in the presence of imposed translayer electrical currents.

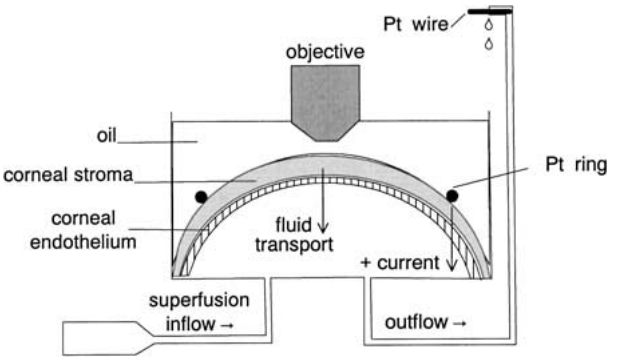

Fig. 1. Schematic diagram of de-epithelialized rabbit corneas (endothelial preparations) in a superfusion chamber (Dikstein & Maurice, 1972) held in a thermal jacket at 36.5°C (not shown).

Methods and Materials

Stromal Thickness of De-epithelialized Rabbit Cornea

Rabbit corneas were obtained from New Zealand albino rabbits (~2 kg). Animal procedures were in accordance with the Guide for the Care and Use of Laboratory Animals (NIH Publication 85-23, revised 1985). Rabbits were euthanized with an overdose of sodium pentobarbital solution injected into the marginal ear vein. The eyes were enucleated immediately using an established technique (Dikstein & Maurice, 1972). The de-epithelialized cornea was mounted in a Dikstein-Maurice chamber (Fig. 1) held in a thermal jacket at 36.5° C. The preparation was viewed with a specular reflection microscope, with which one can detect intense reflections at the stroma-oil and endothelium-fluid interfaces, and can monitor stromal thickness by recording the microscope micrometer position at the interfaces (Dikstein & Maurice, 1972). The endothelial side of the cornea was superfused while the stromal surface was covered with silicone oil.

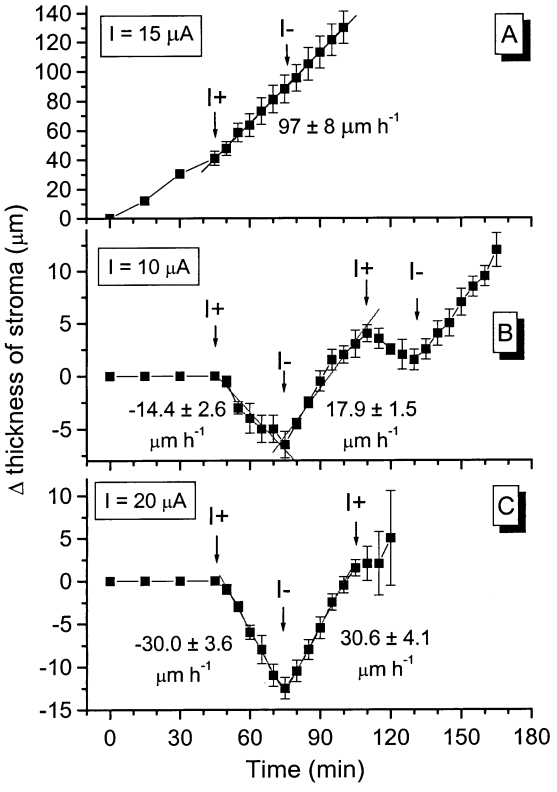

Fig. 2. Current-induced transendothelial fluid movements. It is known that preparations in BH medium remain at baseline thickness for ~30 minutes, and afterwards increase in thickness slowly (~6 μm/hr). In the experiments shown, after an initial stabilization period, externally applied electrical currents generate transendothelial fluid movements as evidenced by stromal thickness changes. *I*+, *I*−: positive and negative currents. Here and elsewhere, unless noted, all experiments were performed with the same protocol, which allowed point-by-point averaging. Numbers by the fitted lines denote the values of the slopes (rate of volume flow per unit area has units of velocity, μm/hr). Slope statistics are weighted by the individual point deviations. *A*: corneal stroma with endothelial layer partially removed. *B*, *C*: endothelial preparations; results for *I* values of 10 and 20 μA, respectively.

Endothelial Superfusion

The medium was a bicarbonate-HEPES (BH) Ringer's solution containing (in mmol/l): NaCl 94.1, $NaHCO_3$ 37.0, KCl 3.8, KH_2PO_4 1, $MgSO_4$ 0.8, $CaCl_2$ 1.7, glucose 6.9, and HEPES 20 (pH = 7.4, osmolality = 300 mOsm). The rate of superfusion was 1.4 ml/hr except when solutions were changed (3.5 ml/hr for 5 min), which has been shown adequate (Kuang et al., 2001). In this procedure, changes in stromal thickness correspond biunivocally to transendothelial fluid movements (Dikstein & Maurice, 1972). The normal thickness of the rabbit stroma is ~350 μm; in all species studied, the corneas are kept relatively dehydrated (therefore transparent) by the endothelial fluid transport activity. Such dehydration results in a standing negative (imbibition) pressure; when transport and imbibition (via leak pathways) are in balance, the oil-covered stroma remains at steady-state thickness (cf. initial control periods in Fig. 2). When the stroma swells (above ~450 μm), the imbibition pressure becomes negligible, and maximal rates of transendothelial fluid transport can be determined by either specular microscopy (Dikstein & Maurice, 1972), Ussing-type (Maurice, 1972) or volume-clamp (Fischbarg, Lim & Bourguet, 1977; Li et al., 2001) chambers.

Imposed Transendothelial Currents

In Fig. 1, an arrow (left) shows the direction in which the endothelium transports fluid normally, from stroma to aqueous. To pass a current through the stroma and endothelial layer (Fig. 1), we immersed a ring of platinum wire into the silicon oil and placed it directly in contact with the anterior surface of the stroma. The circuit was closed with another Pt wire in the outlet of the endothelial superfusion line, and current flowed. The voltage distribution on the stromal surface (hence the transendothelial current density) was scanned by making contact on it with a probe mounted on a manipulator; it was homogeneous within 8% (4 preparations; *data not shown*). In our convention, +current goes from the stroma to the aqueous side (the same as spontaneous fluid transport; cf. right arrow, Fig. 1), and vice-versa. Unless specified, the data points in the figures represent the average ± SEM of 4 or more experiments.

Fluid Transport by Volume Clamp (Nanoinjection)

To improve on the time resolution of the specular microscopy method, the rate of fluid transport across rabbit corneal endothelial preparations was monitored by volume clamp. The methodology has been described extensively for the original measurements (Fischbarg et al., 1977a) and for recent adaptations (Fischbarg et al., 1999; Li et al., 2001). To send current, the same Pt ring described was immersed in the solution bathing the apical side, while a Ag-AgCl wire electrode pierced the stopper that closed the basolateral-side chamber. The voltage output of the nanoinjector instrument went to both a chart recorder and to a 2-channel Dataq interface for a computer running the data-acquisition program Windaq (both interface and software from Dataq Instruments, Akron, OH). Current was recorded using the second channel. Data were collected every 0.4 seconds.

Results

Induced Electro-Osmotic Water Flows

Figure 2 (panels *B* and *C*) shows examples of the core of the present results: electrical currents imposed across the preparation in either direction from stroma to aqueous (+*I*) or vice-versa (−*I*) induce corresponding transendothelial fluid movements. Given the known specific resistance of corneal endothelium of ~20 Ω cm^2, (Fischbarg, 1972; Fischbarg & Lim, 1974; Hodson, 1974; Hodson & Miller, 1976), the current clamp we established (0 to ± 15 μA cm^{-2} corresponds to a voltage gradient of 0 to ±300 μV imposed across the endothelium. These values are in the order of those existing spontaneously (open circuit current: 25 μA cm^{-2}; ΔV ~ 500 μV, and up to ~1300 μV in adenosine-stimulated preparations (Lim & Fischbarg, 1981), *see below*).

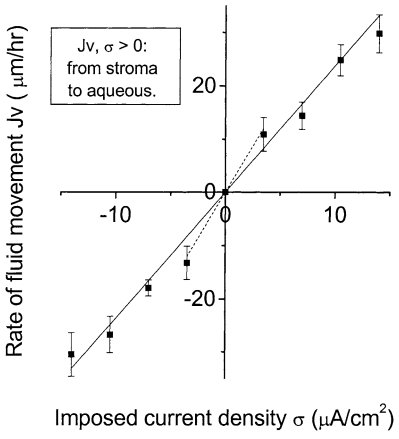

Fig. 3. Fluid movements as a function of the inducing current. The solid line represents a linear fit. The dotted line corresponds to a linear fit for small currents.

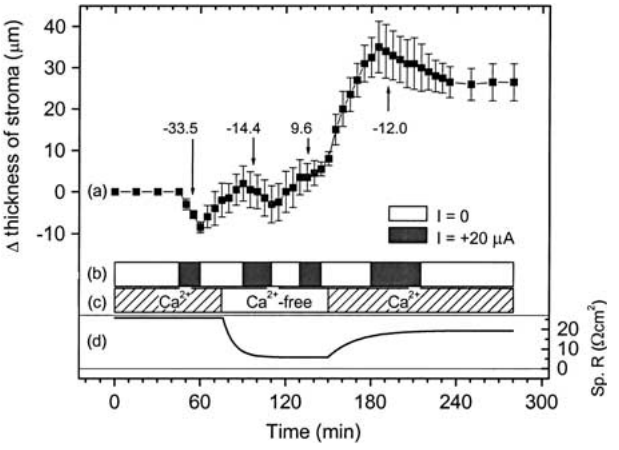

Fig. 4. Electro-osmosis is reduced after nominally Ca^{2+}-free solution (0.1 mM EGTA added) challenge, but partially returns after normal solution is superfused once more. In panel (*a*), each symbol denotes the average ± SEM of 4 experiments done with the same protocol. Current was applied as denoted by the panel (*b*); the values of the slopes obtained (in μm hr^{-1}) are indicated. Panel (*c*) indicates the intervals during which Ca^{2+}-containing (BH) and Ca^{2+}-free solutions were used. Panel (*d*) shows the time course of specific resistance values expected across the layer given resistance values and characteristic time constants determined in separate experiments ($n = 3$) in which endothelial preparations were exposed to Ca^{2+}-free medium.

The induced fluid flow values appear proportional to the currents in both directions. It is understood that the driving forces are actually the voltage gradients imposed across the layer, but we assume that given that the values of the currents we use are in the physiological range, unless noted otherwise, the tissue resistance will remain practically constant. In addition, from inspection of the voltage-current and impedance-resistance characteristics of the corneal endothelium in a prior paper of ours (Figs. 3 and 4 in Lim & Fischbarg, 1981) one can conclude that current is linear with voltage in the current range we utilize. For the work done here, a current clamp is much easier to implement; consequently, in the rest of this paper we simply refer to current-induced fluid movements (cf. also equations (1*a*), (1*b*), and (2) below).

With the low time resolution of this method, the fluid movements begin before the next point is recorded (~5 min, cf. Figs. 2, 4, 6). However, with the much higher temporal resolution procedure described below (cf. Fig. 7), the fluid movements will be seen to begin some 3 seconds after current imposition. Lastly, the effects of currents can be elicited repeatedly within given experiments.

These results are generated only when an intact endothelial layer is in place. Panel *A* of Fig. 2 shows results of control experiments in which a peripheral annulus of the endothelial layer was removed by scraping off the layer with a round scalpel blade. As can be seen, the stroma swells at a fast rate, and the imposition of currents of either sign has no influence on stromal thickness. From these results, and from calculations given in the Appendix (*1*), electro-osmotic coupling at the stroma and chemical changes at the electrodes are not significant factors. For instance, with a positive current of 10 μA (= 7 μA cm^{-2} given a corneal area of 1.43 cm^2), acidification of the stroma and subsequent change in buffering [anion] might result in an artifactual osmotic flow of at most 2 μm hr^{-1}, compared to experimental values of ~15 μm hr^{-1} (Figs. 2 and 3). In addition, such change in rate of fluid movement would take place with a half time of ~19 minutes, which rules out any relation with the fast response of water flow to electrical current application observed here.

Fig. 3 shows that the values of induced fluid flow are overall linear with the currents in the range explored. The slope of the fitted line is 2.37 ± 0.11 μm cm^2 hr^{-1} μA^{-1} ($r = 0.99$). There is also an indication (Fig. 3) that at smaller currents the coupling could be larger, as a line fitted to the points closest to $x = 0$ had a slope of 3.45 ± 0.64 μm hr^{-1} cm^{-1} μA^{-1}. We deal with these subjects in more detail in the Discussion.

The Role of the Junctions

Given the low paracellular resistance of this tissue, the cellular to paracellular fraction i_c/i_p of imposed current traversing the cell is about ~ 1% (Rp~20 Ω cm^2; $Rcell \sim 2Rm \sim 2$ KΩ cm^2; $i_c/i_p = Rp/(Rp + Rcell)$, cf. Fig. 10) (Fischbarg, 1972; Fischbarg & Lira, 1974; Hodson, 1974; Hodson & Miller, 1976). This points to the paracellular pathway as the likely site for the coupling. To investigate this in more detail, we exposed endothelial preparations to Ca^{2+}-free (plus 1 mM EDTA or 0.1 mM EGTA) solutions, a procedure well known to reversibly induce

junctional opening (Kaye, Hoefle & Donn, 1973). We also know (*unpublished data*) that after challenge with Ca^{2+}-free solutions, the endothelial resistance decreases exponentially with a characteristic time of 7.5 ± 1.3 minutes, and upon return to Ca^{2+}-containing medium it recovers partially (up to 75%) with a characteristic time of 19.6 ± 1.2 minutes. Fig. 4 shows the results of the EGTA series; results with EDTA (*not shown*) were very similar. In standard medium, imposition of +current (min 45) results in stromal thinning, while turning off the current results in stromal swelling towards the former steady-state value. Before it reaches that level, Ca^{2+}-free solution is introduced (min 75), and swelling continues. At this point, renewed imposition of current (min 90) results in some thinning, albeit with reduced coupling ratio. To be noted, this reduced coupling ratio is generated when the resistance would be much reduced (panel *d*). This is consistent with the fact that, given the current clamp imposed, the voltage across the coupling sites would have decreased as well, and with it the driving force for electro-osmosis (cf. Eq. 1*a* below). While still in Ca^{2+}-free solution, new imposition of current (min 130) still results in residual electro-osmotic coupling, as it results in a slight reduction of the rate of swelling. After current is turned off (min 145), the stroma begins to swell rapidly, indicating definite junctional opening. At about that point (min 150), Ca^{2+} is reintroduced, and resistance begins to increase. As the recovery of the resistance is nearly complete (panel *d*), re-imposition of current (min 180) induces thinning after a 5-min delay, suggesting partial recovery of electro-osmotic coupling (with a reduced coupling ratio). Upon cessation of current (min 215), thinning continues driven by the spontaneous fluid transport activity, but stabilizes at a level higher than that before Ca^{2+}-free challenge, indicating that the rate of fluid transport has decreased. These results are consistent with electro-osmosis across intercellular junctions.

Spontaneous Fluid Transport and Electro-Osmosis

We explored whether the spontaneous fluid secretion by the endothelium (rather than the current-induced fluid movements) presented characteristics attributable to electro-osmosis. In relatively simple cases, the electrical field E is connected with the velocity of electro-osmotic fluid movement u by the Helmholtz-Smoluchowski equation (Hunter, 1981; Kruyt, 1952; Ohshima & Furusawa, 1998; Tikhomolova & Kemp, 1993):

$$\zeta = -(\eta u)/(\varepsilon\varepsilon_0 E) \tag{1a}$$

where ζ is the zeta or electrokinetic potential (the important characteristic of the surface, or membrane in our case), the viscosity of water, $\varepsilon = 81$ is the dielectric constant for water, and ε_0 is the permittivity of free space. Another frequently used form of the Helmoltz-Smoluchowski expression is that derived by Saxen and cited by Kruyt (1952). This derivation utilizes Ohm's Law in the form:

$$E = \Delta\psi/L_{ep} = I/\kappa A,$$

where L_{ep} is the length of the electro-osmotic pathway, A its cross-sectional area, and κ is the conductivity, and arrives at:

$$\zeta = -(\eta\kappa u)/(\varepsilon\varepsilon_0 i), \tag{1b}$$

where i is the current density, $i = I/A$. For experiments with corneal preparations, it is convenient to work with the experimentally used parameters I and Q, Q being the volume flow $Q = A\ u$.
Solving for Q one has:

$$Q = -(\zeta\varepsilon\varepsilon_0 I)/(\eta\kappa). \tag{2}$$

Hence, given equal currents, electro-osmotic flow should increase as the electrolyte in the medium is diluted (and κ is decreased), and vice versa.

As Fig. 5 shows, as the osmotic gradients are imposed, the preparation reacts as one would expect, with stromal volume shifts entirely attributable to osmosis across the endothelial layer. However, in the second phase, after the osmotic transients end, fluid transfer across the endothelium is driven by endothelial transport. For this phase, our results are in qualitative agreement with the prediction of the concentration-dependence implicit in the Helmholtz-Smoluchowski equation (assuming constant current for all conditions). Always with reference to Fig. 5, after baseline values were obtained at [NaCl] = 94.1, spontaneous transendothelial fluid transport increased when [NaCl] was reduced to 78.3 mM (Fig. 5, curve *4*) and decreased when [NaCl] was increased to 110 mM (Fig. 5, curve *2*). Our results for curves *2* and *4* are similar to some results from another laboratory (Ruberti, 1998) in the same preparation. In contrast, if the solution was made hypertonic to the same degree by sucrose (instead of salt) addition, no effect was seen on the rate of fluid transport (Fig. 5, curve *3*). The dilution of NaCl did not affect the presence of current-induced fluid movements; reduction of [NaCl] (from 94.4 to 78.3, or 17%; replaced by sucrose) resulted only in a small increase in the rate of movement induced by $+I$ (from 24.8 to 27.2 μm/hr, or 10%; *data not shown*). In the case of curve *1*, the exposure to low [NaCl] during the stabilization period appears to damage the cells. Subsequent hypotonic challenge does not elicit the expected transient (as seen in curve *4*), and instead the preparation swells uncontrollably.

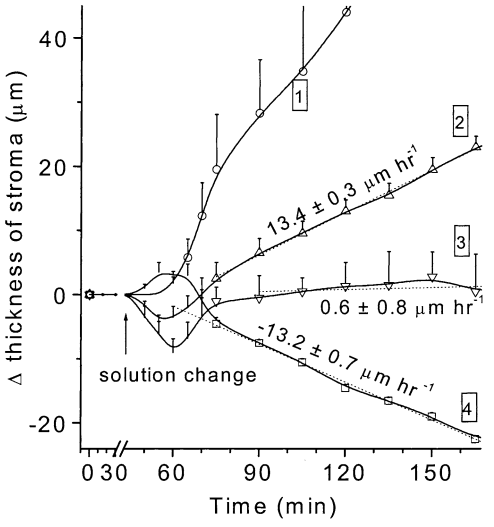

Fig. 5. Effects of medium [NaCl] and osmolarity on rate of fluid transport. After 70 min, the rate of fluid transport depends on [NaCl] but not on osmolarity. For the intervals following solution changes, symbols are omitted for clarity. Solutions were: *A*, standard solution (standard [NaCl]). In the other solutions, most elements were as in *A*, except for (in mM): *B*, NaCl 78.3, sucrose 29 (isotonic; low NaCl, compensated with sucrose); *C*, [NaCl] 110, sucrose 0 (10% hypertonic; high [NaCl]). *D*, NaCl 78.3, sucrose 58 (10% hypertonic; std. [NaCl] plus sucrose added), *E*, NaCl 78.3, sucrose 0 (10% hypotonic; low [NaCl]). $N = 4$ each curve. Curves correspond to the following transitions: (1) $B \rightarrow E$; (2) $A \rightarrow C$; (3) $A \rightarrow D$; (4) $A \rightarrow E$.

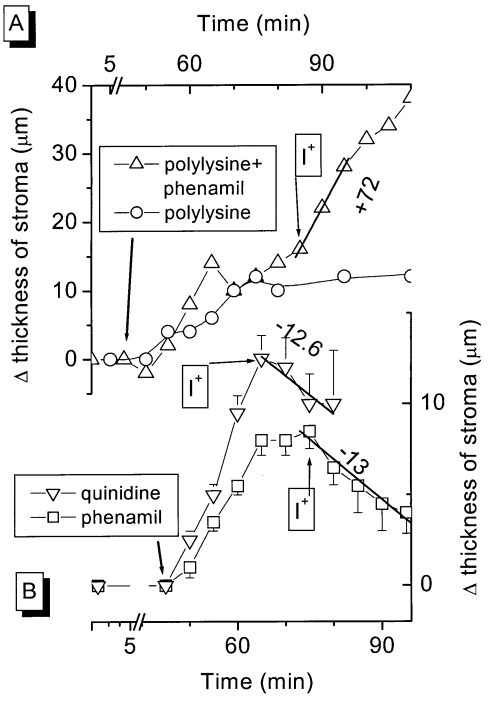

Fig. 6. Current-induced fluid movements in the presence of phenamil, polylysine, and quinidine. Agents were added at the times marked by the arrows. Panel (*A*): Circles represent the effect of adding polylysine (MW 1000; 0.4 mg/ml); single experiment representative of 3. Triangles show the effect of the addition of polylysine (same MW and cone.) plus phenamil (1 μM), followed by challenge with $I = +15$ μA. single experiment representative of 3. Panel (*B*): Squares, addition of 1 μM phenamil followed by challenge with $I = +10$ μA. Inv. triangles, addition of quinidine (300 μM) followed by challenge with $+20$ μAM. In both panels, the thicker lines correspond to fitted slopes for current induced fluid movements; numbers indicate the slopes in μm/hr.

In the second phase, curves *2–4* in Fig. 5 are noteworthy in an important respect, namely, they show three different modes of transendothelial fluid transfer: a) normal rate (increased sucrose, curve *3*); b) decreased rate (elevated NaCl, curve *2*); c) and increased rate (reduced [NaCl], curve *4*). This behavior could not have been predicted *a priori*. The simplest and most consistent explanation for the behavior of such curves is that the rate of fluid transport depends on the ambient ionic concentration in a manner consistent with the electro-osmotic hypothesis currently being presented.

In another series of experiments, blocking epithelial Na^+ channels with 1 μM phenamil led to inhibition of fluid transport (Fig. 6*A*, 6*B*), as expected (cf. (Kuang et al., 1993)). Subsequently, application of $+15$ and -15 μA still induced some stromal thinning (Fig. 6*B*) and swelling (*not shown*), respectively. Importantly, Fig. 6*A* shows that after addition of the polycation polylysine (together with 1 μM phenamil), application of positive current results in fluid movement in a direction opposite to that obtained without polylysine (Fig. 6*B*). Similarly to the results with phenamil, blocking K^+ channels with 300 μM quinidine inhibits fluid transport and causes the stroma to begin to swell (Fig. 6*B*). At that point, application of $+20$ μA elicits some electro-osmotic fluid movement in the normal direction of transport, albeit with reduced coupling.

Time Course of Fluid Movements: *a*) Following the Application of Transendothelial Electrical Currents

It may be argued that the currents imposed in our experiments might act in part by inducing solute fluxes, which would ultimately generate salt gradients and osmotic (rather than electro-osmotic) fluid movements. However, such osmotic flow would build up slowly as the salt gradient develops, whereas electro-osmotic movements would be expected to begin immediately. Therefore, we determined the time course of transendothelial fluid movement immediately after imposition of current. We had already determined that in experiments done with a time resolution of one minute (Kuang et al., 1993), fluid movements began as soon as the current was imposed (*unpublished data*). We decided to explore this once more, with a better time resolution.

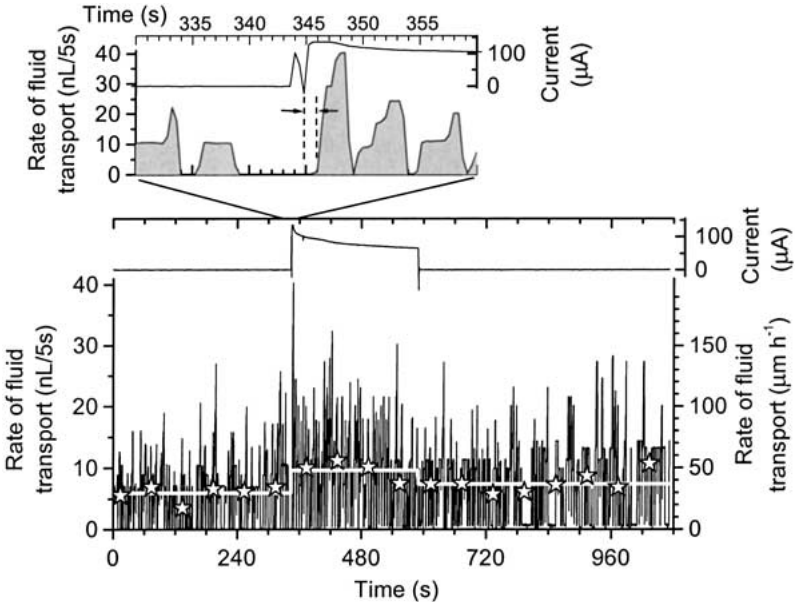

Fig. 7. Time course of the effect of current on the rate of fluid transport across a rabbit endothelial preparation mounted in the volume-clamp chamber. The figure is representative of 19 current steps in 4 preparations. In the bottom panel, positive deflections correspond to fluid transport (from the basolateral to the apical side) against a 3-cm H_2O pressure. The accumulating buffer is reset every 5 seconds, so the height of the deflections corresponds to the amount of nanoliters transported by the endothelium during that interval. The white stars represent averages for one-minute periods. The white lines denote average values for the periods before, during, and after current imposition. The plot at the top of the panel represents the electrical current imposed. The top panel contains a segment of the same data except that the time scale is expanded so as to display the data before and after the current was switched on. The area under the fluid transport curve is grayed for clarity. The arrows delimit the delay between current imposition and the effect on fluid movement. The top panel contains a segment of the same data except that the time scale is expanded so as to display the data before and after the current was switched on. The area under the fluid transport curve is grayed for clarity. The arrows delimit the delay between current imposition and the effect on fluid movement.

The results are exemplified in Fig. 7. As can be seen there in the bottom panel, current-induced fluid movement begins as soon as the current is imposed. As the current decays, so do the fluid movements. The spontaneous rate of fluid transport in this experiment is of the order of those seen in the past using this chamber ($\sim$4.5 μl hr^{-1} cm^{-2}, or 45 μm hr^{-1}, (Fischbarg et al., 1977a)). As these chambers require heavy clamping pressure to prevent fluid leaks, edge damage is presumably high. Perhaps due to that, the nominal currents required to elicit fluid movements are much larger (cf. also our earlier data (Kuang et al., 1993)) than those required in the Dikstein-Maurice chamber (cf. Fig. 2). The current bypassing the preparation via the edge-damage shunt might be a high proportion of the total current sent. As an indication of this, the bottom panel shows that the rate of fluid movement returns to baseline while about half of the original current is still being sent, implying that the current fraction through the endothelium is insufficient to elicit much fluid movement. Still, regardless of such effects, the instantaneous effect on fluid flow is clear. Using the global averages for the three periods of flow (Fig. 7) and the deviations (*not shown*), the changes in rate of flow observed are highly significant ($p \leq 5.7 \times 10^{-25}$ and 4.4×10^{-30} for current imposition and cessation, respectively). Importantly, the top panel amplifies the time scale to show how fast the fluid movement reacts to current imposition. With reference to the interval delimited by the two arrows, the response appears to take place in $\sim$ 1 second. Even if one takes current to begin at the switch-bounce artifact shown, the delay for the response is at most 3 seconds.

Lastly, as Fig. 7 shows, the steady-state rate of fluid transport is larger after current challenge than before. This is reminiscent of the priming effect that osmotic gradients have on fluid transport in this preparation (Fischbarg, Hofer & Koatz, 1980), and thus argues for a) internal consistency of the data, and b) the fact that no lasting damage was inflicted by the current sent.

Time Course of Fluid Movements: *b*) Following the Start of a Theoretical Solute Flux

Although in free solution electrical currents do not result in salt movements, one could theorize that here unique mechanisms in the cells might utilize the energy of current-associated paracellular cation movements to transport anions in the same direction, leading to hypothetical salt displacement and osmosis. As there is no apparent way to determine the time course of such osmotic flows experimentally, we have resorted to a theoretical treatment of convection-diffusion of an idealized electroneutral solute transported across the apical cell membrane into an unstirred layer (cf. Fig. 8). The partial differential equation, and the initial and boundary conditions are given in Fig. 8. We seek solutions for the concentration of solute $C(x,t)$ as a function of the parameter *Pf*. *Js* is the transport of solute across the cell membrane; as we want to reproduce what happens after current is imposed, we assume that *Js* starts at time zero. The accumulation of solute at the boundary ($C(0,t)$) outside the cell induces a local gradient across the membrane, with the consequent osmotic flow *Jv*.

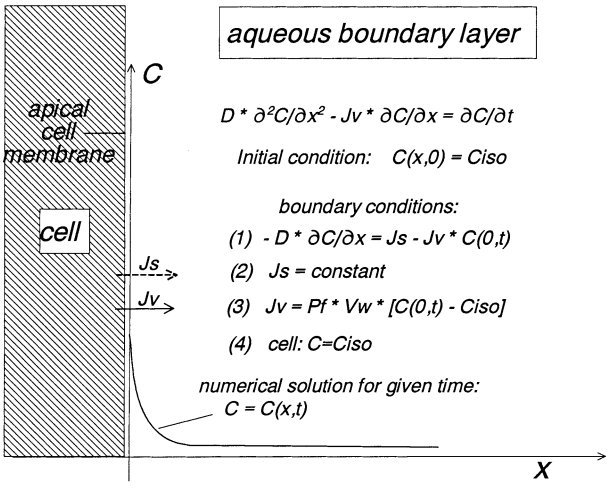

Fig. 8. Scheme of the apical cell membrane and the adjacent aqueous boundary layer. We describe the events at the boundary layer by the convection-diffusion equation, initial and boundary conditions given. At the bottom of the picture, the curve shown illustrates a numerical solution for the concentration of an idealized neutral solute (C, y-coordinate) as a function of the distance to the membrane (x-coordinate) at a given time. C_{iso} (for isotonic concentration) is the cell concentration, assumed equal to that in the bulk of the ambient medium; $C(0,t)$ is the solute concentration at the membrane boundary; Pf is the membrane osmotic permeability, and Vw the water molar volume. At time = 0, solute flux (Js) and a resulting osmotic flow of water (Jv) are established across the membrane as indicated by the arrows, simulating current-induced solute and water flows.

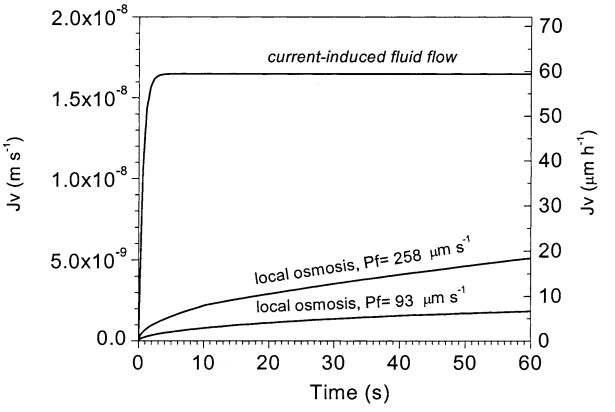

Fig. 9. Solutions of the equations given in the scheme of Fig. 8. The graph represents the transmembrane water flow Jv (uniform for all x) at increasing times after the imposition of the solute flow Js. We used for the calculation a slab of aqueous boundary layer of thickness $x = 20$ μm, and a time step of 0.01 sec. The diffusion coefficient D was 1.5×10^{-5} cm^2 sec^{-1}, corresponding to that of NaCl. C_{iso} was 300 mmol/l. The values of Pf utilized are discussed in the text.

For the osmotic permeability of the apical membrane Pf we consider the following values: 93 μm/sec (Echevarria et al., 1993), a value published for corneal endothelial cell membranes; and 258 μm/sec (Terwilliger & Solomon, 1981), the human erythrocyte Pf (perhaps the cellular Pf value most reliably determined).

To be noted, in our Pf measurements (Echevarria et al., 1993), pCMBS resulted in a 75% decrease in Pf (down to 23 μm/sec). There is another estimate for corneal endothelial apical cell membrane Pf, 460 μm/sec (Sun et al., 2001). However, we believe it constitutes an overestimate, hence do not employ it. In that work (Sun et al., 2001), the baseline Pf resulting from pCMBS inhibition was not reported, but given the 75% inhibition in our results, the baseline Pf would have been 115 μm/sec. This seems exceedingly high, as values in the literature are in the range of only 5 to 20 μm/sec (Flamion & Spring, 1990; House, 1974).

To approximate the case of an endothelial preparation transporting spontaneously, we use our experimentally determined coupling ratio of $r = 2.37$ μm cm^2 hr^{-1} μA^{-1} (Fig. 3) and the value of 25 μA cm^{-2} mentioned above for the circulating open-circuit current. From $Jv = r \times Ioc$, $Jv = 59.25$ μm hr^{-1} (1.65×10^{-8} m sec^{-1}), which is the value that appears in Fig. 9 for the current-induced flow. Figure 9 shows also numerical solutions obtained using the program FlexPDE (PDE Solutions, Antioch, CA). With reference to Fig. 7, the 1-minute average points show that electro-osmotic flows are well established in one minute, so we chose that time interval for the X-axis.

As Fig. 9 shows, in contrast with the immediate rise of the electro-osmotic flow, osmotic flows rise much more slowly, and after one minute would reach only a fraction (11% to 31%) of the current-induced flow. From these results, current-induced solute buildups cannot account for our observations.

Discussion

Our evidence for electro-osmosis across corneal endothelial junctions can be summarized as follows.

1) *Coupling between electrical currents and fluid movements*. Electrical currents externally imposed across the preparation result in corresponding transendothelial fluid movements. As explained in the Results section, it is understood that the driving force for electro-osmotic flow is the voltage gradient imposed. The increase in fluid flow was observed immediately after the imposition of current; from Fig. 7, the delay was between 1 and 3 seconds only. The theoretical treatment covered in Figs. 8 and 9 shows that hypothetical osmotic flows resulting from current imposition would have arisen with a much longer time delay than observed. The presence of current-induced fluid movements with these characteristics constitutes very strong evidence for the existence of electro-osmotic coupling at the endothelial level.

2) *Direction of the fluid movement*. The fluid moves in the direction of transjunctional Na^+ flux across junctions reported to be cation-selective (Lim, Liebovitch & Fischbarg, 1983). Hence, the direction of fluid movement is a separate consistent indication of the presence of electro-osmosis.

3) *Correspondence of the coupling measured with that expected from priorly known spontaneous endothelial electrical activity in the presence of electro-osmosis*. The coupling ratio experimentally found can be used to calculate the rate of fluid transport that the spontaneously circulating endothelial electrical current would originate. The result obtained (59 μm hr^{-1}) agrees very well with known values of corneal deturgescence (Dikstein & Maurice, 1972; Green et al., 1982).

4) *Correspondence with junctional integrity*. The presence of an intact layer of corneal endothelium is necessary for the induced electro-osmosis described here. Damage to this layer completely eliminates the effects of currents on stromal thickness (Fig. 2*A*). Opening the junctions with Ca^{2+}-free solutions reduces electro-osmosis in concert with the decrease in resistance seen across the current-clamped preparation (Fig. 4). Upon return to Ca^{2+}-containing solutions, electro-osmosis partially returns, as does translayer resistance (Fig. 4). Considering evidence that a 98% fraction of the imposed currents traverses the junctions (Fischbarg, 1972; Fischbar & Lim, 1974; Hodson, 1974; Hodson & Miller, 1976), and that the junctions are ~ 39 Å wide (Fischbarg, Warshavsky & Lim, 1977b) and are cation-selective (Lim et al., 1983), this is consistent with the junctions being an important site of electro-osmotic coupling.

5) *Correspondence with cell membrane surface charges*. The polycation polylysine leads to a reversal in the directions in which currents drive the fluid.

6) *Upon varying ambient electrolyte concentration, the rate of fluid transport across corneal endothelium is consistent with Gouy-Chapman and electro-osmotic theories*. Gouy-Chapman theory (Kruyt, 1952) predicts that the surface (or zeta) potential will increase upon dilution of [NaCl] (and vice versa). Furthermore, from Eq. 1, electro-osmotic theory predicts that the rate of fluid movement is proportional to the zeta potential and to the reciprocal of electrical conductance. The present experimental results (Fig. 5) are in qualitative agreement with these predictions. Taken together, our results lead us to propose the model shown schematically in Fig. 10. Arguments for this proposal are discussed in what follows.

The Coupling Ratio—Comparison with Prior Data

The overall coupling ratio found (cf. Fig. 3) was: r = 2.37 ± 0.11 μm cm^2 hr^{-1} μAmp^{-1}). In this connection, it is known that the endothelium maintains a

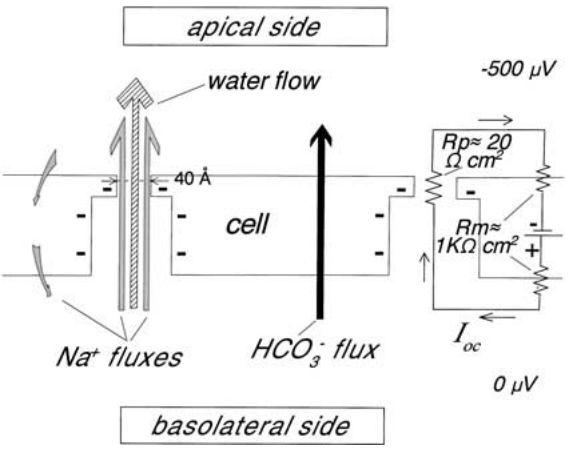

Fig. 10. Electro-osmotic fluid flow: a schematic description of the routes for electrical currents and ionic fluxes described in the text. I_{oc} is the spontaneously circulating open-circuit current (I_{oc} = 25 μA cm^{-2}), resulting from an electromotive force of 500 μV driving current through a paracellular resistance Rp (~20 Ω cm^2). The flux pattern and the potential difference given apply only to the open-circuit condition (no currents imposed). Electro-osmotic coupling would take place at negatively charged cell membranes lining the paracellular spaces and intercellular junctions. The transjunctional Na^+ fluxes shown represent cation fluxes in the electrical double-layer region.

potential difference, PD, of 500 μV (Fischbarg, 1972; Hodson, 1974) and has an Rp of 20 Ω cm^2 (Hodson & Miller, 1976; Lim & Fischbarg, 1979, 1981), hence it must function as a source of an "open circuit" constant current I_{oc} = 25 μA cm^{-2} circulating across the leaky intercellular junctions and back through the cells (Fig. 10). From r and Ioc, we can calculate a rate of fluid transport Jv as: $Jv = r \times I_{oc}$ = 2.37 μm cm^2 hr^{-1} $\mu A^{-1} \times 25$ μA cm^{-2} = 59 μm hr^{-1}. This fits very well with known rates of transendothelial fluid transport; spontaneous rates of corneal deturgescence of around 60 μm hr^{-1} are routinely observed in swollen preparations (Green et al., 1982). The most consistent explanation for such agreement is that the endothelial spontaneous fluid transport is due to its cell-generated current driving fluid by electro-osmosis in the same way as imposed currents do in our results.

There is an indication that coupling could be even more efficient at smaller applied currents. As Fig. 3 shows, the data points near x = 0 (Fig. 3) fall on a line of steeper slope (3.45 ± 0.64 (μm hr^{-1} cm^2 μA^{-1}). With reference to Fig. 10, a conceivable explanation might be that the imposed electric field has the potential capability to drag electrolytes (mostly Na^+) and water quite efficiently across the paracellular route, but for this to result in electroneutral salt transfer, anions (mostly HCO_3^- must be able to follow immediately. As the anion route includes saturable transporters in the cell membranes, the anion flux would limit the rate of fluid transport at higher current densities.

Electro-Osmosis and Osmotic Equilibration

The osmolarity of the transported fluid can be calculated, albeit approximately. We use for the fluid flow the experimental value given above, $Jv = 60$ μm hr^{-1}. We assume such fluid is isotonic, hence its osmolarity would be equal to C_{iso}, or 300 mOsm/L. The flux of transported salt is: $Js = Jv \times C_{iso} = 1.8$ μmol hr^{-1} cm^{-2}. Using the equivalent circuit of Fig. 10, this salt flux corresponds to an open circuit current of: $I_{oc} = 1/2 \times Js \times F = 24$ μA cm^{-2}. The factor of 1/2 arises from the fact that, by electroneutrality, the recirculating current corresponds to equal fluxes of both anions and cations. As can be seen, the value of I_{oc} arrived at in this manner is very close to that of 25 μA cm^{-2} obtained from experimental data. From this argument, the overall coupling ratio is roughly consistent with isotonic transport.

Other Results Consistent with Electro-Osmotic Water Flow Through the Intercellular Junctions

As can be seen in Fig. 6, application of phenamil and quinidine results in inhibition of fluid transport and subsequent stromal swelling. Phenamil would be expected to block Na^+ channels, after which the action of the Na^+ pump would rapidly deplete $[Na^+]_i$ and lead to an arrest of Na^+ extrusion and therefore interruption of the Na^+ current loop. K^+ channel inhibition by quinidine would result in depolarization of the cell membrane and consequently an inhibition of putative apical Na^+-$3HCO_3^-$ cotransport. However, in both cases, imposition of currents elicits fluid movements. Hence, the findings are consistent with junctional integrity being independent of some cellular events in the short run. Together with the rest of the evidence, this points to the junction (rather than cellular channels) as the site for current-fluid coupling. Moreover, polylysine, a polycation known to bind to anionic sites in cell membranes (Torihara, Morimitsu & Suganuma, 1995) and to alter the characteristics of intercellular junctions (McEwan et al., 1993), leads to a reversal in the direction of fluid movement upon challenge with current (Fig. 6*a*, top panel). A possible interpretation is that a reversal in the sign of the net charge present at the junctions would result in a reversal of flow direction, as observed.

Can Hypothetical Current-induced Local Osmosis Explain These Observations?

As mentioned above, it may be argued that the currents imposed would not drive fluid per se but somehow result in salt transfer across the cell layer, generating a concentration gradient that will then drive the fluid by local osmosis. However, a simulation of such process (Figs. 8–9) shows that local osmosis would be insufficient as the osmotic flow would not arise instantaneously, but instead would build up with a relatively slow time course of characteristic times between 40 sec and 32 min (Fig. 9). This contrasts with our observations that the flow begins within 1–3 seconds after the current is imposed (Fig. 7).

Type of Electro-Osmosis Present

Our observations have been discussed in terms of generic classical electro-osmosis, and the Helmholtz-Smoluchowski equation has been used to illustrate some aspects of the results. Still, those equations were developed for a hollow capillary, which is different from a paracellular pathway in an epithelium. It is also doubtful that Schmid-type electro-osmosis can account for these observations, as the junctions have an estimated width of ~40 Å (Fig. 10), which is larger than the estimated Debye length for our case (about 8 Å). Hence, we are developing a novel treatment for the possible physicochemical events that might take place at the paracellular pathway (manuscript in preparation).

A Model Proposed: Paths for Electrical Currents, Water, and Electrolyte Fluxes

Fig. 10 shows the routes for the imposed external currents and for the postulated local open-circuit recirculating current I_{oc}. Electrogenic mechanisms such as anion transport (from basolateral to apical) and the Na^+ pump (from apical to basolateral) may contribute to generate the known transendothelial potential difference of some 500 μV. As mentioned above, this potential difference drives the spontaneously circulating open circuit current across the paracellular resistance, resulting in $I_{oc} = 25$ μA cm^{-2}. In a simple approximation, the paracellular limb for I_{oc} corresponds to cations carrying the current (say Na^+). The transcellular limb has two components: a) anions (say HCO_3^-) moving from basolateral to apical, and Na^+ traversing the cell in the opposite direction, both adding up to carry the return current. This transcellular Na^+ flux may enter the cell via Na^+ channels; there is evidence for their presence in these cells (Kuang et al., 1993; Mirshahi et al., 1999). In this scheme, as required by electroneutrality, the transcellular anion flux is equal to the non-recirculating portion of the paracellular cation flux; this results in translayer salt transfer. As mentioned above, water flow would result from electro-osmosis across the junctions. In this connection, in the formulation of Eqs. 1 and 2 above, we have chosen to present the current explicitly (rather than the voltage) to underline the fact that the cells behave as current sources. A more comprehensive account of the ionic fluxes and current across this epithelium will be presented in a future manuscript currently under preparation.

Can Electro-Osmosis be a General Mechanism?

Some qualitative observations are consistent with the hypothesis advanced here. The fact that fluid transport takes place only in epithelia with leaky junctions is obviously in line with the ideas of this paper. In this regard, there is an interesting comparison: across rabbit corneal epithelium in vitro, a tight epithelium (specific resistance: 6–12 KΩ cm^2, (Marshall & Klyce, 1983)), fluid transport is negligible (0.13 μl hr^{-1} cm^{-2}, (Klyce, 1977)). However, in SV40-immortalized corneal epithelial cell layers cultured on permeable supports, the specific resistance is instead relatively low (184 Ω cm^2), and such layers transport fluid (5.2 μl hr^{-1} cm^{-2} (H. Yang et al., 2000)). There are other instances in the literature that can be termed consistent with our findings. Notably, the laboratories of G. Whittembury (Whittembury et al., 1988) and A. E. Hill (Shachar-Hill & Hill, 1993) have maintained steadfastly over the years that fluid transport across *Necturus* gallbladder is paracellular, and intestinal absorption of nutrients has been attributed to paracellular solvent drag (Madara & Pappenheimer, 1987). In addition, T. Zeuthen has carefully documented that transepithelial fluid transport rates across the gallbladder are larger in dilute solutions (Zeuthen, 1996). Our recalculation (Fig. *A1*) of such results shows that they are quite consistent with electro-osmosis. Lastly, a discussion as to whether fluid movement across kidney proximal tubule is paracellular or transcellular has seasawed, but there is evidence (Tripathi & Boulpaep, 1988) that water moves through both cellular and paracellular pathways in this epithelium.

On the other hand, there are at least two main uncertainties that need to be addressed to admit that this could be a general mechanism. Electroneutral fluid transport across rabbit gallbladder would militate against generality; there is evidence for such electroneutrality (Gelarden & Rose, 1974) and against it (Frederiksen & Leyssac, 1977). Another uncertainty concerns the sign of the charges in the tight junction; for example, an absorptive epithelium following "Rehm's rule" (blood side positive), such as the kidney proximal tubule, would have to have its junctions positively charged so that the transjunctional current would be carried by anions for the observed fluid absorption to take place electro-osmotically. There is a report consistent with this (Anagnostopoulos, 1975), but little else is apparently known in this area.

Conclusions

As mentioned in the introduction, electro-osmosis has been explored considerably less than local osmosis in epithelial physiology. Yet the present results cannot be termed a total surprise. The ideas of Lyslo and Ussing have been already mentioned, as was the fact that we ourselves reported corneal transendothelial fluid movements qualitatively consistent with electro-osmosis but at a lower coupling ratio (Kuang et al., 1993). We hope that the present experimental findings will bring renewed attention to the possibility of electro-osmosis underlying fluid transport.

This research was supported by NIH Grant EY06178, and by Research to Prevent Blindness, Inc. We thank Drs. Michael Field and Martin Blank for helpful comments. The FlexPDE program we utilized is available upon request.

Appendix

1. Current-related Putative Shift in Stromal Concentration

We examine the case of an imposed current I_1 of 10 μA. The corresponding ionic flux is:

$$\Phi_1 = I_1/F = 0.104 \text{ nmol sec}^{-1}.$$

The volume of the stroma (v_s) is the area of the cornea (A_c = 1.43 cm^2) × the height of the stroma (h_s = 350 μm):

$$v_s = A_c \times h_s = 50.1 \ \mu\text{l}.$$

It is not clear whether the pH change in the vicinity of the electrode can affect $[HCO_3^-]$ in the stroma. For argument, we will determine what would be the maximum of such effect. If acidification decreases $[HCO_3^-]$, the rate of change (r_1) of the stromal $[HCO_3^-]$ is:

$$r_1 = \Phi_1/v_s = 2.07 \times 10^3 \text{ nmol sec}^{-1}\text{l}^{-1}.$$

The initial (bulk) stromal concentration of HCO_3^- (B_s) is 37 mmol/l. The total mass of bicarbonate (B^-) in the stroma (MB_s) is:

$$MB_s = B_s \times v_s = 1.85 \times 10^{-6} \text{ mol}.$$

The fractional rate of change of B^- (r_{chB}) is

$$r_{chB} = \Phi_1/MB_s = 3.36 \times 10^{-3} \text{ min}^{-1}.$$

For a typical 15-minute period of recordings, the maximum change is:

$$\Delta t_1 = 15 \text{ min}; \Delta 15 = r_{chB} \times \Delta t_1 = 0.05.$$

Hence, the maximum change in B_s, $M\Delta B_s$ (equal to the putative gradient across the endothelium) would be:

$$M\Delta B_s = B_s \times \Delta 15 = 1.86 \text{ mmol l}^{-1}.$$

The average gradient during that time is:

$$\text{Avgrad} = M\Delta B_s/2 = 0.93 \text{ mmol/l}.$$

Using the correction below for HCO_3^- permeability, the corrected gradient is:

$$\text{Avgr\_corr} = 1.44/2 = 0.72 \text{ mmol l}^{-1}.$$

The transendothelial Pf is 31.5 μm sec^{-1} (Liebovitch, Fischbarg & Koatz, 1981).
Hence, the osmotic flow J_{v_artif} generated by that gradient would be:

$$J_{v\_artif} = \text{Pf} \times \text{Vw} \times \text{Avgr\_corr} = 2.17 \ \mu\text{m hr}^{-1},$$

to be compared with typical displacements of 15 μm/hr obtained with 10 μA currents.

Time-Course for the Putative Change in Concentration

The bulk $[HCO_3^-]$ (CB) is: $CB = B_s$. The current-induced HCO_3^- efflux (J_{seff}) for the entire A_c is: $J_{seff} = 1.03 \times 10^{-10}$ mol sec^{-1}. The endothelial permeability to bicarbonate (PB) can be separately estimated as:

$PB = 2.1 \times 10^{-5}$ cm sec^{-1}.

For convenience, we define coefficients:

$\alpha = J_{seff}/v_s; \qquad \beta = PB/h_s; \qquad \gamma = \alpha + \beta \times CB$

The $[HCO_3^-]$ time course ($C(t)$) is given by:

$C(t) = (\gamma/\beta) \times (1 - e^{-\beta \cdot t}) + CB \times e^{-\beta \cdot t}$,

from which the half-time is: $0.693/\beta = 19.3$ min.
Graphically, it is (y-scale: mmol; x-scale: sec)

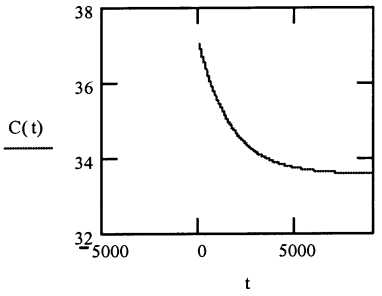

Amplifying, the 15-min change,

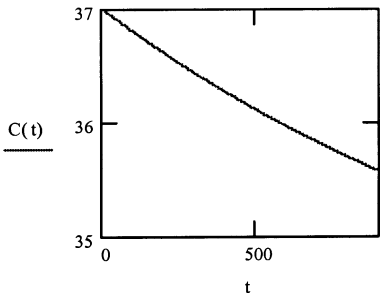

Analytically, the $[HCO_3^-]$ after 15 minutes would be:
$C(900 \text{ sec}) = 35.56$ mmol l^{-1}, for a $[HCO_3^-]$ shift of: $37 - 35.56 = 1.44$ mmol l^{-1}, the value used above.

2. Recalculation of Data in the Literature Yields Results Consistent with Electro-osmosis

T. Zeuthen has carefully documented that transepithelial fluid transport rates across the gallbladder are larger in dilute solutions (Zeuthen, 1996). His data are shown in the main graph of Fig. *A1*. We have recalculated his data, plotting the abscissa as 1/osmolarity, which makes that axis proportional to the specific electrical resistance of the solutions. The results (shown in the inset to Fig. *A1*) are consistent with the inverse relation between fluid movement and conductance that appears, for example, in the Helmholtz-Smoluchowski equation (Eq. 2).

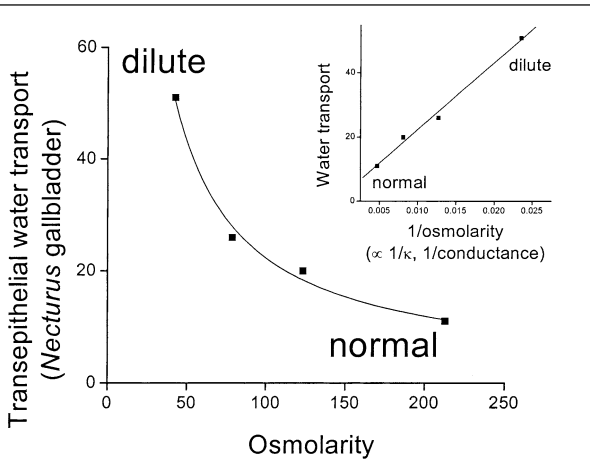

Fig. A1. Data plotted from a book on water transport (Fig. 7.4, Zeuthen, 1996; reproduced with permission). The curve represents a hyperbolic fit ($y = b + K/x$). *Inset*: Same data, replotted with the different X-scale given and a least-squares linear fit ($r = 0.996$).

References

Anagnostopoulos, T. 1975. Anion permeation in the proximal tubule of Necturus kidney: the shunt pathway. *J. Membrane Biol.* **24:**365–380

Deen, P.M.T., Verdijk, M.A.J., Knoers, N.V.A.M., Wieringa, B., Monnens, L.A.H., van Os, C.H., van Oost, B.A. 1994. Requirement of human renal water channel aquaporin-2 for vasopressin-dependent concentration of urine. *Science* **264:**92–95

Dikstein, S., Maurice, D.M. 1972. The metabolic basis of the fluid pump in the cornea. *J. Physiol.* **221:**29–41

Echevarria, M., Kuang, K., Iserovich, P., Li, J., Preston, G.M., Agre, P., Fischbarg, J. 1993. Cultured bovine corneal endothelial cells express CHIP28 water channels. *Am. J. Physiol.* **265:**C1349–C1355

Fischbarg, J. 1972. Potential difference and fluid transport across rabbit corneal endothelium. *Biochim. Biophys. Acta* **228:**362–366

Fischbarg, J., Diecke, F.P., Kuang, K., Yu, B., Kang, F., Iserovich, P., Li, Y., Rosskothen, H., Koniarek, J.P. 1999. Transport of fluid by lens epithelium. *Am. J. Physiol.* **276:**C548–C557

Fischbarg, J., Hofer, G.L., Koatz, R.A. 1980. Priming of the fluid pump by osmotic gradients across rabbit corneal endothelium. *Biochim. Biophys. Acta* **603:**198–206

Fischbarg, J., Lim, JJ. 1974. Role of cations, anions and carbonic anhydrase in fluid transport across rabbit corneal endothelium. *J. Physiol.* **241:**647–675

Fischbarg, J., Lim, J.J., Bourguet, J. 1977a. Adenosine stimulation of fluid transport across rabbit corneal endothelium. *J. Membrane Biol.* **35:**95–112

Fischbarg, J., Warshavsky, C.R., Lim, J.J. 1977b. Pathways for hydraulically and osmotically-induced water flows across epithelia. *Nature* **266:**71–74

Flamion, B., Spring, K.R. 1990. Water permeability of apical and basolateral cell membranes of rat inner medullary collecting duct. *Am. J. Physiol.* **259:**F986–999

Frederiksen, O., Leyssac, P.P. 1977. Effects of cytochalasin B and dimethylsulphoxide on isosmotic fluid transport by rabbit gallbladder in vitro. *J. Physiol.* **265:**103–118

Gelarden, R.T., Rose, R.C. 1974. Electrical properties and diffusion potentials in the gallbladder of man, monkey, dog, goose and rabbit. *J. Membrane Biol.* **19:**37–54

Green, K., Lindorme, P.S., Bowman, K.A., Huff, J.W., Alderman, N. 1982. Pharmacological modification of rabbit corneal endothelial transport and permeability. *Curr. Eye Res.* **2:**791–796

Hemlin, M. 1995. Fluid flow across the jejunal epithelia in vivo elicited by d-c current: effects of mesenteric nerve stimulation. *Acta Physiol. Scand.* **155:**77–85

Hill, A.E. 1975. Solute-solvent coupling in epithelia: an electro-osmotic theory of fluid transfer. *Proc. R. Soc. Lond. B. Biol. Sci.* **190:**115–134

Hill, A.E. 1980. Salt-water coupling in leaky epithelia. *J. Membrane Biol.* **56:**177–182

Hodson, S. 1974. The regulation of corneal hydration by a salt pump requiring the presence of sodium and bicarbonate ions. *J. Physiol.* **236:**271–302

Hodson, S., Miller, F. 1976. The bicarbonate ion pump in the endothelium which regulates the hydration of the rabbit cornea. *J. Physiol.* **263:**563–577

House, C.R. 1974. Water transport in cells and tissues. Edward Arnold Ltd., London

Hunter, R.J. 1981. Zeta Potential in Colloid Science: Principles and Applications. Academic Press, New York

Kaye, G.I., Hoefle, F.B., Donn, A. 1973. Studies on the cornea. 8. Reversibility of the effects of in vitro perfusion of the rabbit corneal endothelium with calcium-free medium. *Invest. Ophthalmol.* **12:**98–113

Klyce, S.D. 1977. Enhancing fluid secretion by the corneal epithelium. *Invest. Ophthalmol. Vis. Sci.* **16:**968–973

Kruyt, H.R. 1952. Colloid Science. Elsevier, New York

Kuang, K., Cragoe, E.J., Fischbarg, J. 1993. Fluid transport and electroosmosis across corneal endothelium. *In:* Proc. Alfred Benzon Symposium 34, "Water transport in leaky epithelia." Ussing, H.H., Fischbarg, J., Sten Knudsen, E., Hviid Larsen, E., Willumsen, N.J., editors, pp. 69–79. Munksgaard, Copenhagen

Kuang, K., Li, Y., Wen, Q., Wang, Z., Li, J., Yang, Y., Iserovich, P., Reinach, P.S., Sparrow, J., Diecke, F.P.J., Fischbarg, J. 2001. Corneal endothelial Na^+-K^+-$2Cl^-$ cotransporter: molecular identification, location, and contribution to fluid transport. *Am. J. Physiol.* **280:**C491–C499

Li, Y., Kuang, K., Yerxa, B., Wen, Q., Rosskothen, H.D., Fischbarg, J. 2001. Rabbit conjunctival epithelium transports fluid, and $P2Y_2$ receptor agonists stimulate Cl^- and fluid secretion. *Am. J. Physiol.* **281:**C595–C602

Liebovitch, L.S., Fischbarg, J., Koatz, R. 1981. Osmotic water permeability of rabbit corneal endothelium and its dependence on ambient concentration. *Biochim. Biophys. Acta* **646:**71–76

Lim, J.J., Fischbarg, J. 1979. Intracellular potential of rabbit corneal endothelial cells. *Exp. Eye Res.* **28:**619–626

Lim, J.J., Fischbarg, J. 1981. Electrical properties of rabbit corneal endothelium as determined from impedance measurements. *Biophys. J.* **36:**677–695

Lim, J.J., Liebovitch, L.S., Fischbarg, J. 1983. Ionic selectivity of the paracellular shunt path across rabbit corneal endothelium. *J. Membrane Biol.* **73:**95–102

Lyslo, A., Kvernes, S., Garlid, K., Ratkje, S.K. 1985. Ionic transport across corneal endothelium. *Acta Ophthalmol.* (*Copenh.*) **63:**116–125

Madara, J.L., Pappenheimer, J.R. 1987. Structural basis for physiological regulation of paracellular pathways in intestinal epithelia. *J. Membrane Biol.* **100:**149–164

Marshall, W.S., Klyce, S.D. 1983. Cellular and paracellular pathway resistances in the "tight" Cl^-- secreting epithelium of rabbit cornea. *J. Membrane Biol.* **73:**275–282

Mathai, J.C., Mori, S., Smith, B.L., Preston, G.M., Mohandas, N., Collins, M., van Zijl, P.C.M., Zeidel, M.L., Agre, P. 1996. Functional analysis of aquaporin-1 deficient red cells: the Colton-null phenotype. *J. Biol. Chem.* **271:**1309–1313

Maurice, D.M. 1972. The location of the fluid pump in the cornea. *J. Physiol.* **221:**43–54

McEwan, G.T., Jepson, M.A., Hirst, B.H., Simmons, N.L. 1993. Polycation-induced enhancement of epithelial paracellular permeability is independent of tight junctional characteristics. *Biochim. Biophys. Acta* **1148:**51–60

McLaughlin, S., Mathias, R.T. 1985. Electro-osmosis and the reabsorption of fluid in renal proximal tubules. *J. Gen. Physiol.* **85:**699–728

Mirshahi, M., Nicolas, C., Mirshahi, S., Golestaneh, N., o'Hermies, F., Agarwal, M.K. 1999. Immunochemical analysis of the sodium channel in rodent and human eye. *Exp. Eye Res.* **69:**21–32.

Moore, M., Ma, T., Yang, B., Verkman, A.S. 2000. Tear secretion by lacrimal glands in transgenic mice lacking water channels AQP1, AQP3, AQP4 and AQP5. *Exp. Eye Res.* **70:**557–562

Nielsen, S., Smith, B.L., Christensen, E.I., Knepper, M.A., Agre, P. 1993. CHIP28 water channels are localized in constitutively water-permeable segments of the nephron. *J. Cell Biol.* **120:**371–383

Ohshima, H., Furusawa, K. 1998. Electrical Phenomena at Interfaces. Marcel Dekker, New York

Pasquale, L.R., Mathias, R.T., Austin, L.R., Brink, P.R., Ciunga, M. 1990. Electrostatic properties of fiber cell membranes from the frog lens. *Biophys. J.* **58:**939–945

Preston, G.M., Carroll, W.B., Guggino, W.B., Agre, P. 1992. Appearance of water channels in *Xenopus* oocytes expressing red cell CHIP28 protein. *Science* **256:**385–387

Preston, G.M., Smith, B.L., Zeidel, M.L., Moulds, J.J., Agre, P. 1994. Mutations in aquaporin-1 in phenotypically normal humans without functional CHIP water channels. *Science* **265:**1585–1587

Rae, J.L., Mathias, R.T. 1985. The physiology of the lens. *In:* The Ocular Lens. Structure, Function, and Pathology. Maisel, H., editor, pp. 93–122. Marcel Dekker, New York

Ruberti, J.W. 1998. Experimental and computational investigation of corneal transport properties. Ph. D. Thesis, Tulane University, New Orleans

Shachar-Hill, B., Hill, A.E. 1993. Convective fluid flow through the paracellular system of *Necturus* gall-bladder epithelium as revealed by dextran probes. *J. Physiol.* **468:**463–486

Spring, K.R. 1998. Routes and mechanism of fluid transport by epithelia. *Annu. Rev. Physiol.* **60:**105–119

Spring, K.R., Paganelli, C.V. 1972. Sodium flux in *Necturus* proximal tubule under voltage clamp. *J. Gen. Physiol.* **60:**181–201

Sun, X.C., Alien, K.T., Xie, Q., Stamer, W.D., Bonanno, J.A. 2001. Effect of AQP1 expression level on CO_2 permeability in bovine corneal endothelium. *Invest. Ophthalmol. Vis. Sci.* **42:**417–423

Terwilliger, T.C., Solomon, A.K. 1981. Osmotic water permeability of human red cells. *J. Gen. Physiol.* **77:**549–570

Tikhomolova, K.P., Kemp, TJ. 1993. Electro-osmosis. E. Horwood, New York

Torihara, K., Morimitsu, T., Suganuma, T. 1995. Anionic sites on Reissner's membrane, stria vascularis, and spiral prominence. *J. Histochem. Cytochem.* **43:**299–305

Tripathi, S., Boulpaep, E.L. 1988. Cell membrane water permeabilities and streaming currents in Ambystoma proximal tubule. *Am. J. Physiol.* **255:**F188–F203

Ussing, H.H., Eskesen, K. 1989. Mechanism of isotonic water transport in glands. *Acta Physiol. Scand.* **136:**443–454

Whittembury, G., Malnic, G., Mello-Aires, M., Amorena, C. 1988. Solvent drag of sucrose during absorption indicates paracellular

water flow in the rat kidney proximal tubule. *Pflügers Arch.* **412:**541–547

Yang, B., Ma, T., Verkman, A.S. 2001. Erythocyte water permeablility and renal function in double knockout mice lacking aquaporin-1 and aquaporin-3. *J. Biol. Chem.* **276:**624–628

Yang, H., Reinach, P.S., Koniarek, J.P., Wang, Z., Iserovich, P., Fischbarg, J. 2000. Fluid transport by cultured corneal epithelial cell layers. *Br. J. Ophthalmol.* **84:**199–204

Zeuthen, T. 1996. Molecular mechanisms of water transport. R.G. Landes, Austin, Texas